
Human Pathologic Correlation with PET in Ischemic and Nonischemic Cardiomyopathy

Jonathan J. Berry, John M. Hoffman, Charles Steenbergen, Jay A. Baker, Carey Floyd, Peter Van Trigt, Michael W. Hanson and R. Edward Coleman

Division of Cardiology, Department of Medicine, Section of Nuclear Medicine, Department of Radiology, Department of Pathology, Department of Surgery, Duke University Medical Center, Durham, North Carolina

To assess the correlation between myocardial perfusion, metabolism and histologic findings in patients with cardiomyopathy, we evaluated myocardial perfusion and metabolism using positron emission tomography (PET) with $^{13}\text{NH}_3$ (ammonia) and ^{18}F (fluoro-2-deoxy-glucose) in nine patients prior to undergoing orthotopic cardiac transplantation. Four patients had ischemic cardiomyopathy (ISCM) and five had nonischemic cardiomyopathy (NISCAM). Normalized circumferential profile analyses of representative mid-ventricular perfusion and metabolism PET images were performed for each patient. A corresponding mid-ventricular transaxial slice was obtained from the formalin fixed explanted heart and processed for routine histology. Hematoxylin-eosin stained and Masson trichrome stained sections were evaluated and the percentage of the slice occupied by infarct was determined planimetrically at 10-degree intervals in a circumferential manner. A significant correlation was found between circumferential normalized PET count density profile of perfusion and metabolism in both the ischemic and nonischemic groups (ISCM range $r = 0.65-0.75$; NISCAM range, $r = 0.70-0.87$). Furthermore, there was a correlation in the ISCM group between the extent of matched perfusion/metabolism defects and transmural infarct involvement ($r = 0.66-0.88$). PET perfusion and metabolic data closely correlate with pathologic infarction in human hearts of ischemic cardiomyopathy patients.

J Nucl Med 1993; 34:39-47

The ability to distinguish nonviable or infarcted myocardial tissue from either normal or viable ischemic myocardial tissue continues to be a clinical challenge. Accurate and reliable quantification of irreversibly damaged myocardium has both therapeutic and prognostic importance (1-6).

Numerous methods of sizing and localizing the extent of irreversible myocardial injury exist, including enzymatic (6-14), electrocardiographic (15-21), scintigraphic (22-

34), echocardiographic (35-37) and magnetic resonance imaging (38-40) methods, all of which are fraught with difficulties which have precluded widespread clinical use. Positron emission tomography (PET), utilizing a variety of metabolic and perfusion tracers, is an imaging modality which shows promise in accurately addressing the important question of tissue viability. Marshall et al. (41) used ^{18}F -2-fluorodeoxyglucose (FDG) and ^{13}N -ammonia in patients with myocardial infarction to distinguish ischemic-viable from infarcted-nonviable tissue by comparing regional count density with a normal population data base and defined PET infarction as a matched defect in perfusion and metabolism. This concept has been validated in animal models (42-44) and has been used prospectively to accurately predict postrevascularization return of function in reversibly injured, viable tissue and the lack of functional benefit to infarcted segments (45,46).

Pathologic validation of the PET criteria used for the identification of infarcted myocardium was performed in this study using $^{13}\text{NH}_3$ for myocardial perfusion and ^{18}F FDG for viability imaging in patients with cardiomyopathy who subsequently had orthotopic cardiac transplantation.

METHODS

Patients on the cardiac transplantation list at Duke University Medical Center underwent PET imaging with $^{13}\text{NH}_3$ and ^{18}F FDG prior to orthotopic cardiac transplantation in order to determine the extent of myocardial infarction. The study population consisted of nine patients [four with ischemic cardiomyopathy (ISCM) and five with nonischemic cardiomyopathy (NISCAM)] who had perfusion and metabolic images obtained prior to cardiac transplantation. ISCM and NISCAM are defined pathologically as the presence or absence respectively of histologic myocardial infarction. The average time between PET imaging and transplantation was 39 days (range = 7 to 87 days). There were no clinical events suggestive of myocardial infarction in any patient between the date of PET scanning and transplantation. Clinical and demographic characteristics are listed in Table 1.

Imaging Protocol

Patients were positioned in the gantry of the ECAT III PET tomograph (CTI, Knoxville, TN) and a transmission rectilinear scan was performed utilizing a ^{68}Ga external ring source. This scan allowed localization of the cardiac silhouette for correct

Received Jun. 4, 1992; revision accepted Aug. 17, 1992.

For reprints or correspondence contact: John M. Hoffman, MD, Department of Radiology, Division of Nuclear Medicine, Duke University Medical Center, Box 3949, Durham, NC 27710.

TABLE 1
Clinical Characteristics

Patient no.	M/FM	Age (yr)	MI (Y/N)	CABG (Y/N)	EF (%)	# Vess. Dis.	EKG	G/F
1	F	48	Y	Y	18	3	Ant. MI/LVH/RBBB	F
2	M	51	Y	Y	14	2	Ant. MI	G
3	M	46	Y	Y	10	3	Ant. MI/RBBB	F
4	M	52	Y	N	10	3	LVH	G
5	M	41	N	N	4	1	LVH	G
6	F	62	N	N	23	0	LBBB	F
7	M	34	N	N	13	0	Ant. MI	G
8	F	33	N	N	14	0	Ant./Sept. MI/LVH	F
9	F	56	N	N	14	1	LBBB	G

Ant. = anterior; CABG = coronary artery bypass grafting; EF = ejection fraction; F = fasted; G = glucose loaded; Inf. = inferior; LBBB = left bundle branch block; LVH = left ventricular hypertrophy; MI = myocardial infarction; RBBB = right bundle branch block; Sept. = septal; Vess. Dis. = $\geq 75\%$ stenosis in any epicardial coronary artery.

positioning to obtain the tomographic transmission and emission scans. The collimators were set at 65 mm giving a full width at half maximum (FWHM) resolution of 16 mm. Three transmission planes were acquired for 10 min (two direct planes, one cross-plane) for attenuation correction. Ten millicuries (370 MBq) of $^{13}\text{NH}_3$ were administered intravenously and data were acquired for 10 min after 3 min of equilibration. Immediately following the perfusion study acquisition, 10 mCi (370 MBq) of ^{18}FDG were injected intravenously. After a 30 min period for accumulation, emission data were acquired for 10 min. Patients were studied in the fasting state (≥ 12 hr fasting) ($n = 4$) or after receiving 50 g of oral glucose (Glucola) 30 min prior to the injection of ^{18}FDG ($n = 5$).

PET Image Analysis

Perfusion and metabolic PET images were reconstructed, attenuation corrected, and transferred onto a SUN III workstation where a circumferential region of interest (ROI) count density profile was constructed using an interactive program. The initial ROI (containing 21 pixels) was assigned to the intersection of the right ventricular free wall, the interventricular septum and the left ventricular anterior wall at the mid ventricular level (Fig. 1A). Contiguous ROIs of the same size were then placed in a clockwise fashion around the circumference of the perfusion and metabolic PET images. By assigning the first ROI as 0 degrees, the radial angle was automatically computed by the program for the line joining the geometric center of the left ventricular cavity with the center of the ROI. This method of analysis allowed paired data of mean count density of all pixels within a given ROI and radial angle to be generated. The circumferential count density profile for each ROI was then normalized for the ROI with the highest mean count density. In addition, the PET images were interpreted by two experienced observers without benefit of clinical information. The interpretation of either ISCM or NISCM was based on the uniformity of tracer distribution in the myocardium.

Pathology

The hearts were removed at the time of transplantation and placed in phosphate-buffered formalin for approximately 48 hr to allow fixation. A physician from the PET laboratory with the study pathologist oriented the heart in its anatomic position. While viewing the transaxial PET images, they selected a mid-

ventricular transaxial slice corresponding to a PET imaging level. This slice was then divided into eight or nine cross sections which were processed for routine histology. Two paraffin embedded sections were prepared from each tissue block; one was stained with hematoxylin and eosin, the other with a Masson trichrome stain, and the circumferential transmural extent of the infarcted tissue was determined (Figs. 1B-C). Beginning at the same starting point of 0 degrees established in the PET ROI analysis, the percent of noninfarcted tissue was determined by planimetry in each 10-degree sector (Fig. 1B). Histologic myocardial infarction was defined as dense, confluent areas of fibrosis with loss of normal myocardial architecture.

Data Analysis

Pair-wise correlation, using Spearman rank order correlation coefficients (for nonparametric data), was used to correlate normalized ^{18}FDG and $^{13}\text{NH}_3$ ROI count density with percent non-infarcted tissue at similar radial locations (± 5 degrees) around the circumference of the myocardium.

RESULTS

There were four patients in the ISCM group and five patients in the NISCM group. The average age of the ISCM group was 49 yr (range 46-52) and for the NISCM group 45 yr (range 33-62). All patients in the ISCM group had a history of one or more documented myocardial infarctions and three of four patients had EKG criteria (Q-waves) of myocardial damage. The mean EF was 13% for both the ISCM and NISCM groups (Table 1). No history of prior myocardial infarctions were present in the patients with NISCM, although two patients had anterior precordial Q-waves. All patients with ISCM had significant coronary artery disease pathologically ($\geq 75\%$ stenosis in at least one epicardial coronary artery). None of the five patients with NISCM had angiographic evidence of significant ($> 75\%$) coronary artery disease, but two patients had pathologic evidence of significant one-vessel coronary artery disease. Neither of these patients had a totally occluded vessel.

Pathologic examination of all hearts with NISCM revealed no gross or histologic evidence of myocardial in-

PET/Pathology Correlation

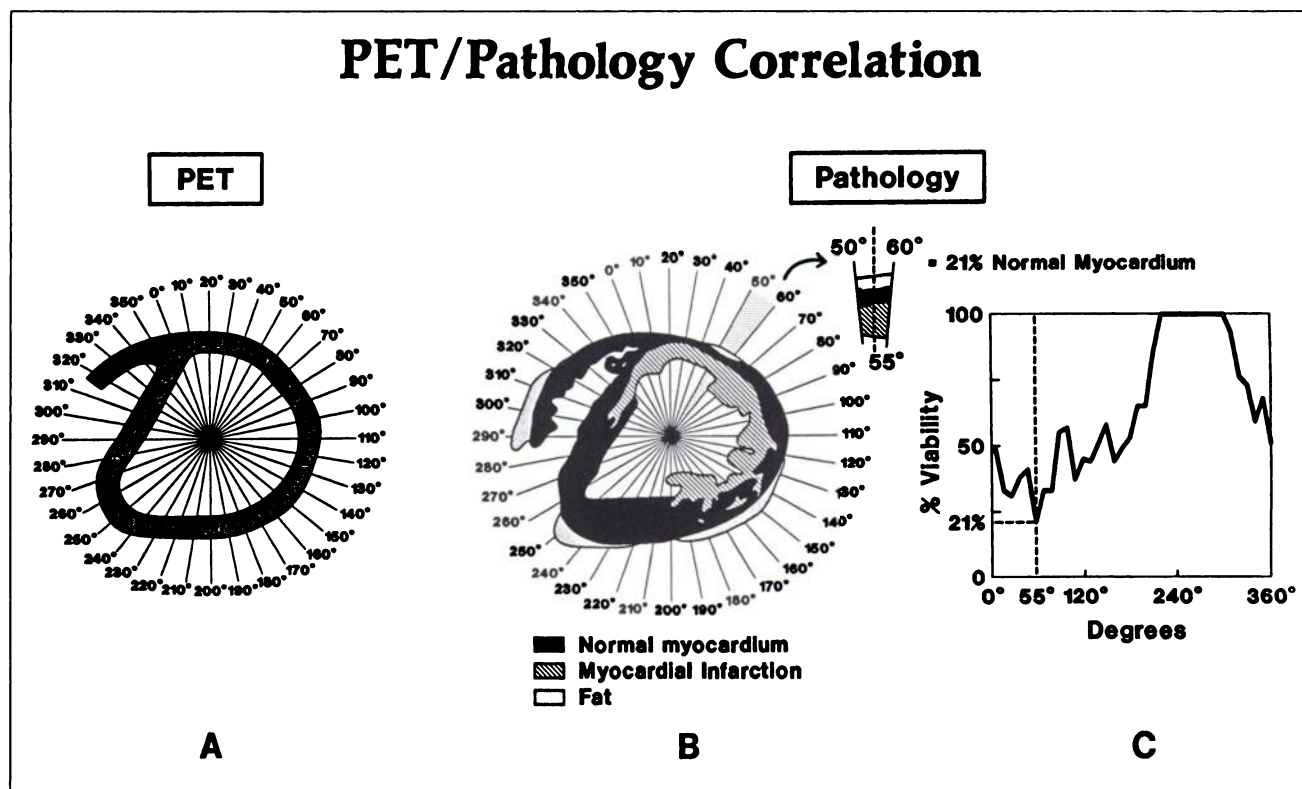


FIGURE 1. ROI analysis of PET image (A) and pathology (B). Note the assignment of the initial ROI (labeled 0°) at the intersection of the right ventricular free wall, the interventricular septum, and the left ventricular anterior wall. (C) Quantitative circumferential histopathological analysis of a midventricular, transaxial slice of myocardium and the extent of transmural involvement by the infarction process is planimetrically quantitated at 10-degree intervals in a clockwise, circumferential manner to correspond to the PET ROI.

faction. There was evidence of interstitial and perivascular fibrosis in most cases. In contrast to this, all hearts in the ISCM group showed extensive areas of myocardial infarction with varying degrees of transmural involvement. All infarcts were old (>6 mo) histologically and characterized by extensive areas of confluent fibrosis with thinning of the affected area.

In the NISCM group, the percent of normal tissue (circumferential pathologic analysis) was uniformly 100% in all hearts; therefore, a correlation could not be performed between PET and pathologic data. However, the correlation between the perfusion and metabolism circumferential profile analysis was significant ($r \geq 0.70$; $p < 0.001$) for all hearts, indicating a very close coupling between perfusion and metabolism. Figure 2 shows an example of the count density profile for Patient 5 (NISCM). The perfusion and metabolism ROI profiles are closely coupled in all segments. Of particular interest is the decline in count density in the infero-lateral, inferior and infero-septal walls (between 180–270 degrees).

All patients in the ISCM group had perfusion and metabolic images which could be evaluated, except for Patient 4 who had an uninterpretable FDG image because of persistent blood-pool activity. Patients 1, 2 and 3 had excellent correlation between PET perfusion/metabolism

count density profiles and pathology (Table 2). Figure 3 shows the perfusion and metabolism PET images of Patient 1 with an arrow pointing to the initial ROI at 0 degrees. Figure 4A shows the schematic representation of the gross pathology and Figure 4B shows the corresponding PET pathology correlation for Patient 1. This individual had an extensive nontransmural anterior infarct with a total left anterior descending and left circumflex coronary artery occlusion and anterior Q-waves on EKG. A close correlation is seen between the extent of transmural pathologic involvement with the PET count density profile.

Figures 5A and B show the pathology schematic and the PET pathology correlation of a patient with a lateral and infero-posterior myocardial infarction. There are two small areas which are transmurally involved with fibrosis but probably appear no different on the count profiles because of partial volume effects.

The location of Q-waves on EKG correlated well with the pathologic location of myocardial infarction in all patients with ISCM. In the patients with NISCM however, two patients had significant Q-waves in the anterior precordial leads indicative of an anterior myocardial infarction. These patients had no evidence for significant coronary artery disease by coronary angiography. Furthermore, these two patients had no evidence of myocardial damage

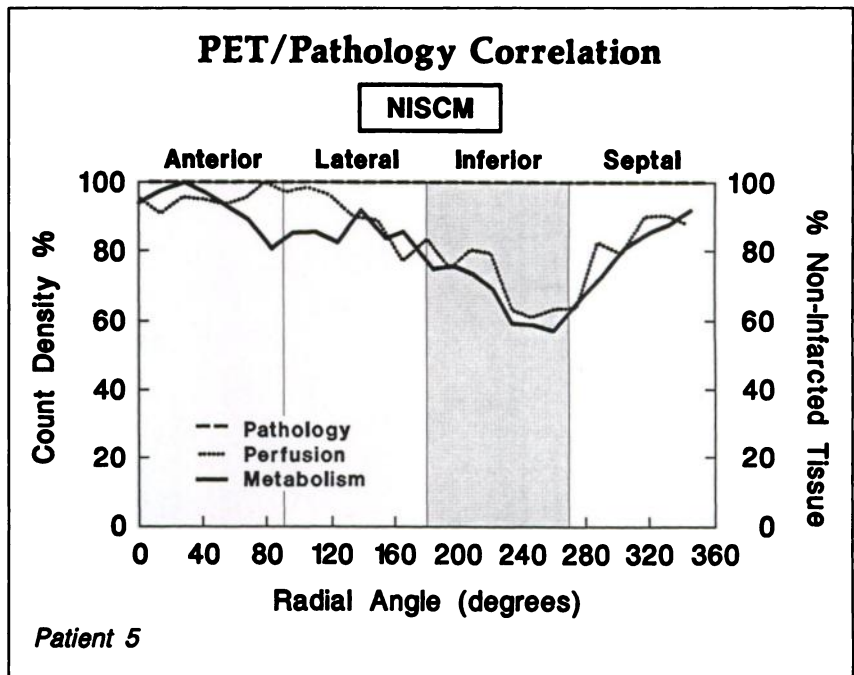


FIGURE 2. PET ROI pathology correlative graphical representation of a patient with nonischemic cardiomyopathy. Dotted line across the top represents 100% non-infarcted tissue by pathology. Circumferential perfusion and metabolism PET count profile shows the tight coupling between perfusion and metabolism. Decline in counts in the inferior wall is discussed in detail in text.

pathologically and had normal PET count density profiles in the anterior wall.

DISCUSSION

Myocardial viability is a diagnostic problem which has been studied by a multitude of noninvasive modalities. Critical decisions regarding patient management depend on differentiating viable, ischemic, and possibly jeopardized myocardium from nonviable, irreversibly damaged tissue. Risk stratification and prognostic information (1-6) are provided by assessing the amount of infarcted tissue and its impact on regional and global LV function. Designing effective means of reducing myocardial infarct size (47-48) and preserving jeopardized myocardium requires a method of distinguishing viable from nonviable tissue. This distinction becomes even more crucial when formulating a revascularization strategy involving myocardial

segments which display contractile dysfunction that may represent either irreversibly injured tissue or acutely stunned and/or chronically hibernating (49-52) but reversibly dysfunctional tissue.

Scintigraphic methods using ^{201}Tl , $^{99\text{m}}\text{Tc}$ -pyrophosphate (22-34) and ^{111}In -antimyosin antibodies (53-57) have been used to address the question of viability but each method has limitations. Further innovations to address the question of myocardial viability have been described that combine scintigraphic imaging modalities such as dual isotope imaging with $^{99\text{m}}\text{Tc}$ -pyrophosphate and ^{201}Tl (58-61) or ^{111}In -antimyosin antibody and ^{201}Tl (53). These approaches have shown promising results. A fixed ^{201}Tl perfusion defect is thought to represent scar, however, between 20% (62) and 75% (63,64) of persistent ^{201}Tl defects improve after revascularization. Serial or delayed imaging (65-67) or ^{201}Tl reinjection (68-70) may improve the sensitivity and specificity of detecting viable myocardium. Brunken et al. (71) and Tamaki et al. (72) showed ^{18}F FDG metabolic activity by PET in segments with persistent ^{201}Tl perfusion defects, implying that persistent defects may represent severe ischemia in addition to infarction. Thus, persistent defects on ^{201}Tl imaging may overestimate the amount of nonviable tissue. Myocardial infarct size, assessed pathologically in man, correlates fairly well with scintigraphic methods utilizing ^{201}Tl (22) and $^{99\text{m}}\text{Tc}$ -pyrophosphate (23). Other methods have been used for detecting the extent of myocardial damage, such as electrocardiographic QRS scoring (15-21), intervention ventriculography (73), echocardiographic assessment of wall thickening (37), back scatter analysis (74,75), and magnetic resonance imaging (38-40).

PET is a metabolic imaging modality which shows promise in differentiating normal from ischemic and in-

TABLE 2
PET: Path Correlation

Patient no.	IS/NIS	FDG: Path r =	NH ₃ : Path r =	FDG: NH ₃ r =
1	IS	0.82	0.72	0.75
2	IS	0.88	0.60	0.69
3	IS	0.73	0.84	0.65
4	IS	—	0.72	—
5	NIS	—	—	0.74
6	NIS	—	—	0.86
7	NIS	—	—	0.70
8	NIS	—	—	0.87
9	NIS	—	—	0.70

FDG = fluorodeoxyglucose; IS = ischemic; NIS = nonischemic; r = Spearman rank order correlation coefficient.

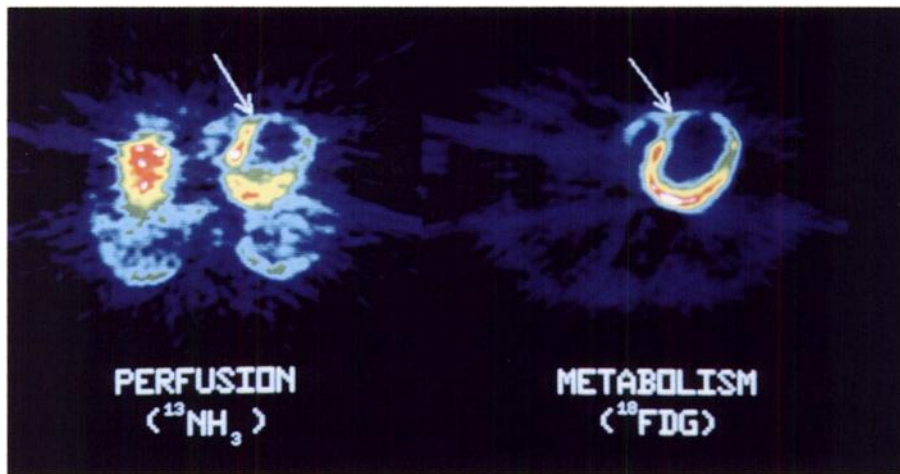


FIGURE 3. PET perfusion (left) and metabolism (right) images of Patient 1 (ISCM). The arrows point to the initial 0-degree ROI assignment at the intersection of the right ventricular free wall, the interventricular septum, and the left ventricular anterior wall.

farcted myocardium. In a canine model of transient (3 hr) ischemia followed by reperfusion, Schwaiger et al. (42) showed that myocardial perfusion using $^{13}\text{NH}_3$ and metabolic activity using ^{11}C -palmitate (CPA) correlated well with the degree of functional recovery at 4 wk and the extent of necrosis found at autopsy. Fluorine-18-deoxyglucose uptake correlated less well with functional recovery. In patients with acute myocardial infarction, studied with PET utilizing $^{13}\text{NH}_3$ and ^{18}FDG within 72 hr after onset of symptoms, segments with a matched reduction in perfusion and metabolism showed no improvement in wall motion at 12 wk, whereas a significant improvement in wall motion occurred in 50% of the segments showing persistent metabolic activity (76). Marshall et al. (41)

utilized PET with ^{18}FDG and $^{13}\text{NH}_3$ to differentiate ischemia from infarction in man. They compared the circumferential profile analysis of patients with a history of acute myocardial infarction to that of a normal data base. Infarction was defined as a matched perfusion and metabolic defect that fell below two standard deviations over a 60-degree sector. Histologic confirmation of this definition has not been shown in humans. Indeed, in a canine model involving a 2-hr left anterior descending coronary artery occlusion followed by reperfusion, Melin et al. (77) showed that ^{18}FDG uptake was associated with viable tissue by TTC staining, while depressed ^{18}FDG uptake indicated irreversible injury. Weiss et al. (78) quantified myocardial infarct size in a chronic canine left anterior descending

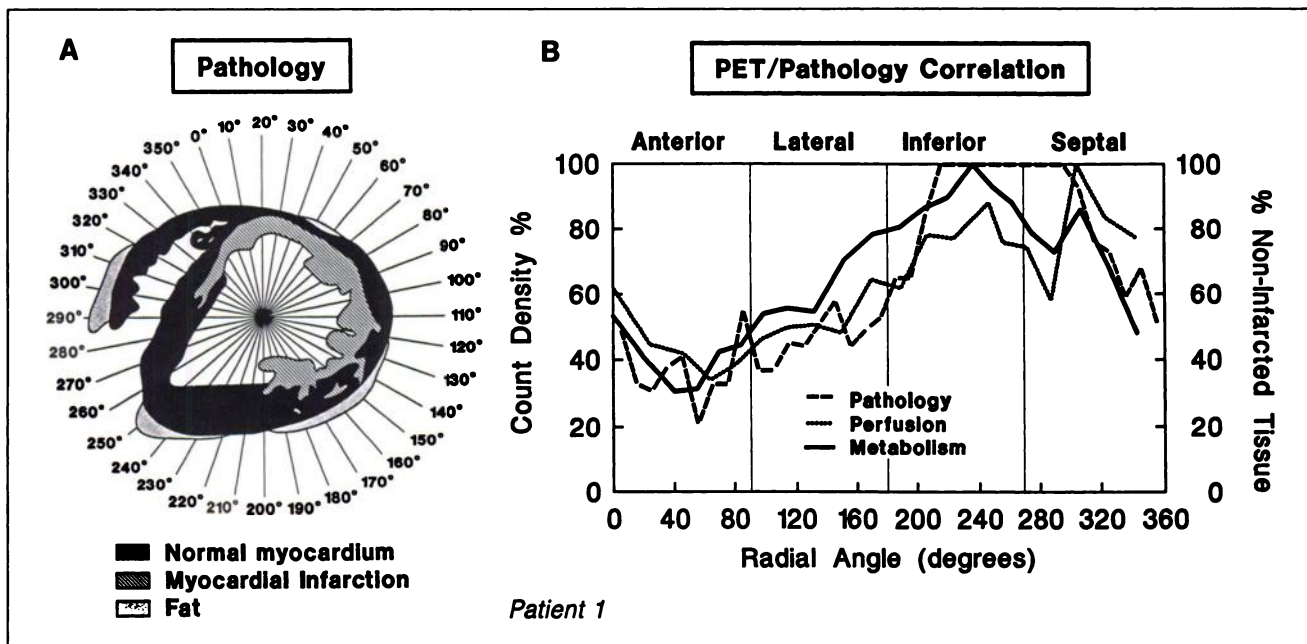


FIGURE 4. (A) Pathology of Patient 1 showing extensive antero-septal, anterior, and antero-lateral nontransmural myocardial infarction. (B) PET pathology correlative circumferential ROI analysis for Patient 1 with ischemic cardiomyopathy. Note the close correlation of PET and pathology corresponding to areas of nontransmural myocardial infarction.

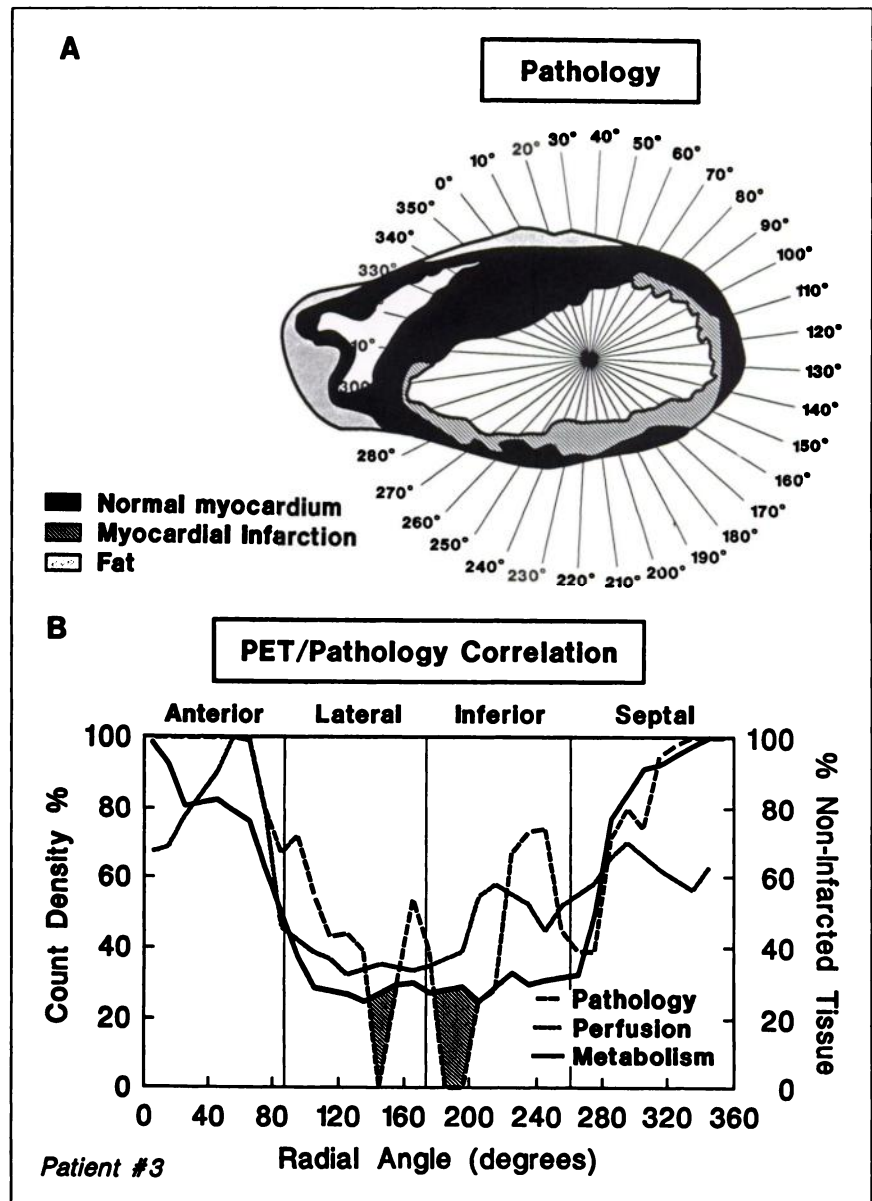


FIGURE 5. (A) Schematic pathological representation of Patient 3 with extensive anterolateral, lateral and infero-posterior myocardial infarction. (B) PET-pathology circumferential correlative ROI analysis of Patient 3. Shaded areas represent transmural extension of fibrosis.

coronary artery occlusion model by PET using ^{11}C -palmitate and found a high correlation between PET estimated infarct size and both histologic and CPK depletion estimates. CPA has also been used with PET in patients with acute myocardial infarction to compare PET derived myocardial infarct size with CPK release (79). PET, using ^{11}C -palmitic acid, has been used to distinguish transmural from non-transmural myocardial infarction (80,81) and ischemic from nonischemic cardiomyopathy (82,83). Ter-Pogossian et al. (79) likewise found a high correlation between PET estimated infarct size and enzymatic (CK-MB) estimates in patients with acute myocardial infarction.

In this study, nine patients (four ISCM, five NISCM) with comparably severe left ventricular dysfunction had histologic correlation of PET perfusion and metabolic data. In the group with ISCM, there was excellent corre-

lation between PET and pathology in all patients.

In the group with NISCM, there was excellent correlation between perfusion and metabolism. In all five hearts, the inferior wall showed diminished perfusion and metabolism. The reason for this apparent decrease is not clear. When compared to circumferential profile analysis of perfusion and metabolism in normal volunteers (unpublished data), a similar matched decrease in count density was observed in the inferior wall. A possible explanation for this finding could be partial volume effect in this segment because of its tangential orientation with the tomographic data acquired with our PET tomograph. Newer PET systems allowing oblique reconstruction (along the short-axis of the heart) may be helpful in determining the true significance of these findings. Marshall et al. (41) showed a similar decrease in perfusion and metabolism using $^{13}\text{NH}_3$ and ^{18}FDG in the inferior segments of their normal

patients. Visual comparison of the perfusion and metabolic PET images of the ISCM group with the NISCM group reveals a homogeneous pattern in the latter and a heterogeneous, segmentally abnormal pattern in the former. Similar findings have been observed in two previous reports (82,83) using ^{11}C -palmitate and PET and in one report using $^{13}\text{NH}_3$ and ^{18}FDG with PET (84). Our findings on the visual interpretations agree with these previous reports, and the patients in our study had pathologic confirmation.

Because of the limited resolution (FWHM = 16mm) of the ^{18}FDG and $^{13}\text{NH}_3$ studies with our tomograph, determination of the transmural extent of infarction is difficult to assess. Three tomographic PET slices were obtained, but oblique reorientation with the long-axis of the heart is not possible with only three imaging planes obtained at a single bed position. Reorientation would permit better evaluation of the inferior wall. The images were obtained in an ungated mode and thus regional asynergy could contribute to apparent differences in regional perfusion and metabolism by PET (85,86). The raw PET data were not adjusted for wall thickness. Areas of chronic infarction exhibit wall thinning which may artifactually diminish PET count density because of partial volume effects (87).

Patients in this study were imaged in either the fasted or glucose loaded state. Metabolic preparation of patients (fasting versus glucose loading) undergoing PET imaging with ^{18}FDG has been shown by Gropler et al. (88) to critically affect the regional distribution of ^{18}FDG myocardial uptake. These differences could affect both visual interpretation of the PET images (89) as well as the quantitative PET/pathology correlation. However, they demonstrated no effect of glucose loading on regional myocardial perfusion. The metabolic state of the patients in this study did not seem to have an effect on the results because the metabolism and perfusion were congruent in every patient. In our series only a single study, however, was compromised by an uninterpretable FDG study.

The ^{18}FDG and $^{13}\text{NH}_3$ studies in patients with ISCM correlated well with pathology. Areas of matched perfusion and metabolic defects on PET corresponded in location to areas of pathologically confirmed infarction. In patients with NISCM, there were no areas of abnormalities on PET and no pathologic evidence of infarction. Since a good correlation was found between a matched perfusion and metabolic defect and irreversible tissue damage pathologically, the matched defects by PET reflect infarcted myocardium.

ACKNOWLEDGMENTS

The authors would like to thank Sandra Bowling and Suzanne Ealy-Romey for their expert secretarial support and John Need PhD, Craig Harris MS, Sharon Hamblen, David Coates and Tom Hawk for technical support. This research was partially supported by NIH SCOR grant P50-HL17760.

REFERENCES

1. Page DL, Caulfield JB, Kastor JA, De Sanctis RW, Sanders CA. Myocardial changes associated with cardiogenic shock. *N Engl J Med* 1971;285:133-137.
2. Alonzo DR, Scheidt S, Post M, Killip T. Pathophysiology of cardiogenic shock: quantification of myocardial necrosis, clinical, pathologic and electrocardiographic correlations. *Circulation* 1973;48:588-596.
3. Geltman EM, Ehsani AA, Campbell MK, Schechtman K, Roberts R, Sobel BE. The influence of location and extent of myocardial infarction on long-term ventricular dysrhythmia and mortality. *Circulation* 1979;60:805-814.
4. Perez-Gonzalez J, Botvinick EH, Dunn R, et al. The late prognostic value of acute scintigraphic measurement of myocardial infarct size. *Circulation* 1982;66:960-971.
5. Holman BL, Goldhaber SZ, Kirsch KM, et al. Measurement of infarct size using single photon emission computed tomography and technetium-99m pyrophosphate: a description of method and comparison with patient prognosis. *Am J Cardiol* 1982;50:503-511.
6. Sobel BE, Bresnahan GF, Shell WE, Yoder RD. Estimation of infarct size in man and its relation to prognosis. *Circulation* 1972;46:640-648.
7. Shell WE, Kjekshus JK, Sobel BE. Quantitative assessment of the extent of myocardial infarction in the conscious dog by means of analysis of serial changes in serum creatinine phosphokinase activity. *J Clin Invest* 1971;50:2614-2625.
8. Roberts R, Henry PD, Sobel BE. An improved basis for enzymatic estimation of infarct size. *Circulation* 1975;52:743-753.
9. Rogers WJ, McDaniel HG, Smith LR, Mantel JA, Russell RO, Rackley CE. Correlation of angiographic estimates of myocardial infarct size and accumulated release of creatine kinase MB isoenzyme in man. *Circulation* 1977;56:199-205.
10. Morrison J, Coromilas J, Munsey D, et al. Correlation of radionuclide estimates of myocardial infarction size and release of creatine kinase-MB in man. *Circulation* 1980;62:277-287.
11. Devries SR, Jaffe AS, Geltman EM, Sobel BE, Abendschein DR. Enzymatic estimation of the extent of irreversible myocardial injury early after reperfusion. *Am Heart J* 1989;117:31-36.
12. Roe CR, Cobb FR, Starmer CF. The relationship between enzymatic and histologic estimates of the extent of myocardial infarction in conscious dogs with permanent coronary occlusion. *Circulation* 1977;55:438-449.
13. Grande P, Hansen BF, Christiansen C, Naestoft J. Estimation of acute myocardial infarct size in man by serum CK-MB measurements. *Circulation* 1982;65:756-764.
14. Hackel DB, Reimer KA, Ideker RE, et al. Comparison of enzymatic and anatomic estimates of myocardial infarct size in man. *Circulation* 1984;70:824-835.
15. Savage RM, Wagner GS, Ideker RE, Podolsky SA, Hackel DB. Correlation of postmortem anatomic findings with electrocardiographic changes in patients with myocardial infarction. *Circulation* 1977;55:279-285.
16. Eisen HJ, Barzilai B, Jaffe AS, Geltman EM. Relationship of QRS scoring system to enzymatic and pathologic infarct size: the role of infarct location. *Am Heart J* 1988;115:993-1001.
17. Seino Y, Staniloff HM, Shell WE, Mickle D, Shah PK, Vyden JK. Evaluation of a QRS scoring system in acute myocardial infarction. Relation to infarct size, early stage left ventricular ejection fraction, and exercise performance. *Am J Cardiol* 1983;52:37-42.
18. Roubin GS, Shen WF, Kelly DT, Harris PJ. The QRS scoring system for estimating myocardial infarct size: clinical, angiographic and prognostic correlations. *J Am Coll Cardiol* 1983;2:38-44.
19. Ideker RE, Wagner GS, Ruth WK, et al. Evaluation of a QRS scoring system for estimating myocardial infarct size: II. Correlation with quantitative anatomic findings for anterior infarcts. *Am J Cardiol* 1982;49:1604-1614.
20. Ward RM, White RD, Ideker RE, et al. Evaluation of a QRS scoring system for estimating myocardial infarct size: IV. Correlation with quantitative anatomic findings for posterolateral infarcts. *Am J Cardiol* 1984;53:706-714.
21. Roark SF, Ideker RE, Wagner GS, et al. Evaluation of a QRS scoring system for estimating myocardial infarct size: III. Correlation with quantitative anatomic findings for inferior infarcts. *Am J Cardiol* 1983;51: 382-389.
22. Wackers FJ, Becker AE, Samson G, et al. Localization and size of acute transmural myocardial infarction estimated from thallium-201 scintiscans: a clinicopathological study. *Circulation* 1977;56:72-78.
23. Poliner LR, Buja M, Parkey RW, Bonte FJ, Willerson JT. Clinicopathologic findings in 52 patients studies by technetium-99m stannous pyro-

- phosphate myocardial scintigraphy. *Circulation* 1979;59:257-267.
24. Mahmarian JJ, Pratt CM, Borges-Neto S, Cashion WR, Roberts R, Verani MS. Quantification of infarct size by ²⁰¹Tl single-photon emission computed tomography during acute myocardial infarction in humans: comparison with enzymatic methods. *Circulation* 1988;78:831-839.
 25. Tamaki S, Murakami T, Kadota K, Kambara H, et al. Effects of coronary artery reperfusion on relation between creatine kinase-MB and infarct size estimated by myocardial emission tomography with thallium-201 in man. *J Am Coll Cardiol* 1983;2:1031-1038.
 26. Tamaki S, Nakajima H, Murakami T, et al. Estimation of infarct size by myocardial emission computed tomography with thallium-201 and its relation to creatine kinase-MB release after myocardial infarction in man. *Circulation* 1982;66:994-1001.
 27. Henning H, Schelbert HR, Righetti A, Ashburn WL, O'Rourke RA. Dual myocardial imaging with technetium-99m pyrophosphate and thallium-201 for detecting, localizing and sizing acute myocardial infarction. *Am J Cardiol* 1977;40:147-155.
 28. Prigent F, Maddahi J, Garcia EV, Satoh Y, Van Train K, Berman DS. Quantitation of myocardial infarct size by thallium-201 single-photon emission computed tomography: experimental validation in the dog. *Circulation* 1986;74:852-861.
 29. Bulkley BH, Silverman K, Weisfeldt ML, Burow R, Pond M, Becker LC. Pathologic basis of thallium-201 scintigraphic defects in patients with fatal myocardial injury. *Circulation* 1979;60:785-792.
 30. Bulkley BH, Hutchins GM, Bailey I, Strauss HW, Pitt B. Thallium-201 imaging and gated cardiac blood pool scans in patients with ischemic and idiopathic congestive cardiomyopathy. A clinical and pathologic study. *Circulation* 1977;55:753-760.
 31. Keyes JW, Leonard PF, Brody SL, Svetkoff DL, Rogers WL, Lucchesi BR. Myocardial infarct quantification in the dog by single-photon emission computed tomography. *Circulation* 1978;58:227-232.
 32. Jansen DE, Corbett JR, Wolfe CL, et al. Quantification of myocardial infarction: a comparison of single-photon emission computed tomography with pyrophosphate to serial plasma MB-creatinine kinase measurements. *Circulation* 1985;72:327-333.
 33. Wolfe CL, Lewis SE, Corbett JR, Parkey RW, Buja LM, Willerson JT. Measurement of myocardial infarction fraction using single photon emission computed tomography. *J Am Coll Cardiol* 1985;6:145-151.
 34. Lewis SE, DeVous MD, Corbett JR, et al. Measurement of infarct size in acute canine myocardial infarction by single-photon emission computed tomography with technetium-99m pyrophosphate. *Am J Cardiol* 1984;54:193-199.
 35. Weiss JL, Bulkley BH, Hutchins GM, Mason SJ. Two-dimensional echocardiographic recognition of myocardial injury in man: a comparison with postmortem studies. *Circulation* 1981;63:401-408.
 36. Wyatt HL, Meerbaum S, Heng MK, Rit J, Gueret P, Corday E. Experimental evaluation of the extent of myocardial dyssynergy and infarct size by two-dimensional echocardiography. *Circulation* 1981;63:607-614.
 37. Lieberman AN, Weiss JL, Jugdutt BI, et al. Two-dimensional echocardiography and infarct size: relationship of regional wall motion and thickening to the extent of myocardial infarction in the dog. *Circulation* 1981;63:739-746.
 38. Caputo GR, Sechlem U, Tscholakoff D, Higgins CB. Measurement of myocardial infarct size at early and late time intervals using MR imaging: an experimental study in dogs. *Am J Radiol* 1987;149:237-243.
 39. Bouchard A, Reeves RC, Crannery G, Bishop SP, Pohost GM. Assessment of myocardial infarct size by means of T2-weighted H Nuclear magnetic resonance imaging. *Am Heart J* 1989;117:281-289.
 40. Johns JA, Leavitt MB, Newell JB, et al. Quantitation of acute myocardial infarct size by nuclear magnetic resonance imaging. *J Am Coll Cardiol* 1990;15:143-149.
 41. Marshall RC, Tillish JH, Phelps ME, et al. Identification and differentiation of resting myocardial ischemia and infarction in man with positron computed tomography, 18F-labeled fluorodeoxyglucose and N-13 ammonia. *Circulation* 1983;67:766-778.
 42. Schwaiger M, Schelbert HR, Ellison D, et al. Sustained regional abnormalities in cardiac metabolism after transient ischemia in the chronic dog model. *J Am Coll Cardiol* 1985;6:336-347.
 43. Schwaiger M, Neese RA, Araujo L, et al. Sustained non oxidative glucose utilization and depletion of glycogen in reperfused canine myocardium. *J Am Coll Cardiol* 1989;13:745-754.
 44. Schelbert HR, Henze E, Phelps ME, Kuhl DE. Assessment of regional myocardial ischemia by positron emission computed tomography. *Am Heart J* 1982;103:588-597.
 45. Tillisch J, Brunken R, Marshall R, Schwaiger M, et al. Reversibility of cardiac wall-motion abnormalities predicted by positron tomography. *N Engl J Med* 1986;314:884-888.
 46. Tamaki N, Yonekura Y, Yamashita K, et al. Positron emission tomography using fluorine-18 deoxyglucose in evaluation of coronary artery bypass grafting. *Am J Cardiol* 1989;64:860-865.
 47. Buja LM, Willerson JT. Infarct size. Can it be measured or modified in humans? *Prog in Cardiovasc Dis* 1987;29:271-289.
 48. Rude RE, Muller JE, Braunwald E. Efforts to limit the size of myocardial infarcts. *Ann Internal Med* 1981;95:736-761.
 49. Braunwald E, Rutherford JD. Reversible ischemic left ventricular dysfunction: evidence for the "hibernating myocardium". *J Am Coll Cardiol* 1986;8:1467-1470.
 50. Rahimtoola SH. The hibernating myocardium. *Am Heart J* 1989;117:211-220.
 51. Kloner RA, Przyklen K, Patel B. Altered myocardial states: the stunned and hibernating myocardium. *Am J Med* 1989; 86(suppl.IA):14-22.
 52. Braunwald E, Kloner RA. The stunned myocardium: prolonged, post-ischemic ventricular dysfunction. *Circulation* 1982;66:1146-1149.
 53. Johnson LL, Lerrick KS, Coromilas J, et al. Measurement of infarct size and percentage of myocardium infarcted in a dog preparation with single, photon emission computed tomography, thallium-201, and indium-111 monoclonal antimyosin Fab. *Circulation* 1987;76:181-190.
 54. Antunes ML, Seldin DW, Wall RM, Johnson LL. Measurement of acute Q-wave myocardial infarct size with single photon emission computed tomography imaging of indium-111 antimyosin. *Am J Cardiol* 1989;63:777-783.
 55. van Vlies B, Bass J, Visser CA, et al. Predictive value of indium-111 antimyosin uptake for improvement of left ventricular wall motion after thrombolysis in acute myocardial infarction. *Am J Cardiol* 1989;64:167-171.
 56. Tamaki N, Yamada T, Matsumori A, et al. Indium-111 antimyosin antibody imaging for detecting different stages of myocardial infarction: comparison with technetium-99m pyrophosphate imaging. *J Nucl Med* 1990;31:136-142.
 57. Jain D, Crawley JC, Lahiri A, Raftery EB. Indium-111 antimyosin images compared with triphenyl tetrazolium chloride staining in a patient six days after myocardial infarction. *J Nucl Med* 1990;31:231-233.
 58. Hashimoto T, Kambara H, Fudo T, et al. Significance of technetium-99m/Thallium-201 overlap on simultaneous dual emission tomography in acute myocardial infarction. *Am J Cardiol* 1988;61:1181-1186.
 59. Sochor H, Schwaiger M, Schelbert HR, et al. Relationship between ²⁰¹Tl, ^{99m}Tc (Sn) pyrophosphate and F-18 2-deoxyglucose uptake in ischemically injured dog myocardium. *Am Heart J* 1987;114:1066-1077.
 60. Schofer J, Speilmann RP, Bromel T, Bleifeld W, Mathey DG. Thallium-201/technetium-99m pyrophosphate overlap in patients with acute myocardial infarction after thrombolysis: prediction of depressed wall motion despite thallium uptake. *Am Heart J* 1986;112:291-295.
 61. Schofer J, Mathey DG, Montz R, Bleifeld W, Stritzke P. Use of dual intracoronary scintigraphy with thallium-201 and technetium-99m pyrophosphate to predict improvement in left ventricular wall motion immediately after intracoronary thrombolysis in acute myocardial infarction. *J Am Coll Cardiol* 1983;2:737-744.
 62. Gibson RS, Watson DD, Taylor GJ, et al. Prospective assessment of regional myocardial perfusion before and after coronary revascularization surgery by quantitative thallium-201 scintigraphy. *J Am Coll Cardiol* 1983;1:804-815.
 63. Liu P, Kiess MC, Okada RD, et al. The persistent defect on exercise thallium imaging and its fate after myocardial revascularization: does it represent scar or ischemia? *Am Heart J* 1985;110:996-1001.
 64. Berger BC, Watson DD, Burwell LR, et al. Redistribution of thallium at rest in patients with stable and unstable angina and the effect of coronary artery bypass surgery. *Circulation* 1979;60:1114-1125.
 65. Kiat H, Berman DS, Maddahi J, et al. Late reversibility of tomographic myocardial thallium-201 defects: an accurate marker of myocardial viability. *J Am Coll Cardiol* 1988;12:1456-1463.
 66. Okada RD, Boucher CA. Differentiation of viable and nonviable myocardium after acute reperfusion using serial thallium-201 imaging. *Am Heart J* 1987;113:241-249.
 67. Pohost GM, Zir LM, Moore RH, McKusick KA, Guiney TE, Beller GA. Differentiation of transiently ischemic from infarcted myocardium by serial imaging after a single dose of thallium-201. *Circulation* 1977;55:294-302.
 68. Bonow RO, Dilsizian V, Cuocolo A, Bacharach SL. Identification of viable myocardium in patients with chronic coronary artery disease and left ventricular dysfunction: comparison of thallium scintigraphy with reinjection and PET imaging with ¹⁸F-fluorodeoxyglucose. *Circulation*

- 1991;83:26-37.
69. Dilsizian V, Smeltzer WR, Dextras R, Bonow RO. Does twenty-four hour delayed imaging following thallium reinjection enhance detection of viable myocardium? [Abstract]. *J Am Coll Cardiol* 1990;15(suppl A):248A.
 70. Dilsizian V, Rocco TP, Freeman N, Smeltzer WR, Bonow RO. Thallium reinjection after stress redistribution imaging improves detection of ischemic myocardium: a qualitative and quantitative SPECT study [Abstract]. *J Am Coll Cardiol* 1990;15(suppl A):147A.
 71. Brunken R, Schwaiger M, Grover-McKay M, Phelps ME, Tillish J, Schelbert HR. Positron emission tomography detects tissue metabolic activity in myocardial segments with persistent thallium perfusion defects. *J Am Coll Cardiol* 1987;10:557-567.
 72. Tamaki N, Yonekura Y, Yamashita K, et al. Relation of left ventricular perfusion and wall motion with metabolic activity in persistent defects on thallium-201 tomography in healed myocardial infarction. *Am J Cardiol* 1988;62:202-208.
 73. Banka VS, Bodenheimer MM, Shah R, Helfant RH. Intervention ventriculography: comparative value of nitroglycerin, post-extrasystolic potentiation and nitroglycerin plus post-extrasystolic potentiation. *Circulation* 1976;53:632-637.
 74. Fitzgerald PJ, McDaniel MD, Rolett EL, Strohhahn JW, James DH. Two-dimensional ultrasonic tissue characterization: backscatter power, endocardial wall motion, and their phase relationship for normal, ischemic, and infarcted myocardium. *Circulation* 1987;76:850-859.
 75. Milunski MR, Mohr GA, Perez JE, et al. Ultrasonic tissue characterization with integrated backscatter: acute myocardial ischemia, reperfusion, and stunned myocardium in patients. *Circulation* 1989;80:491-503.
 76. Schwaiger M, Brunken R, Grover-McKay M, et al. Regional myocardial metabolism in patients with acute myocardial infarction assessed by positron emission tomography. *J Am Coll Cardiol* 1986;8:800-808.
 77. Melin JA, Wijns W, Keyeux A, et al. Assessment of thallium-201 redistribution versus glucose uptake as predictors of viability after coronary artery occlusion and reperfusion. *Circulation* 1988;77:927-934.
 78. Weiss ES, Ahmed SA, Welch MJ, Williamson JR, Ter-Pogossian MM, Sobel BE. Quantification of infarction in cross sections of canine myocardium in vivo with positron emission transaxial tomography and ¹¹C-palmitate. *Circulation* 1977;55: 66-73.
 79. Ter-Pogossian MM, Klein MS, Markham J, Roberts R, Sobel BE. Regional assessment of myocardial metabolic integrity in vivo by positron emission tomography with ¹¹C-labeled palmitate. *Circulation* 1980;61:242-255.
 80. Geltman EM, Biello D, Welch MJ, Ter-Pogossian MM, Roberts R, Sobel BE. Characterization of nontransmural myocardial infarction by positron emission tomography. *Circulation* 1982;65:747-755.
 81. Hashimoto T, Kambara H, Fudo T, et al. Non-Q wave versus Q wave myocardial infarction: regional myocardial metabolism and blood flow assessed by positron emission tomography. *J Am Coll Cardiol* 1988;12:88-93.
 82. Eisenberg JD, Sobel BE, Geltman EM. Differentiation of ischemic from non-ischemic cardiomyopathy with positron emission tomography. *Am J Cardiol* 1987;59:1410-1414.
 83. Geltman EM, Smith JL, Beecher D, Ludbrook PA, Ter-Pogossian MM, Sobel BE. Altered regional myocardial metabolism in congestive cardiomyopathy detected by positron tomography. *Am J Med* 1983;74:773-785.
 84. Mody FV, Brunken RC, Stevenson LW, Nienaber CA, Phelps ME, Schelbert HR. Can positron tomography distinguish dilated from ischemic cardiomyopathy? [Abstract]. *Circulation* 1988;78(suppl II):92.
 85. Yamashita K, Tamaki N, Yonekura Y, et al. Quantitative analysis of regional wall motion by gated positron emission tomography: validation and comparison with left ventriculography. *J Nucl Med* 1989;30:1775-1786.
 86. Parodi O, Schelbert HR, Schwaiger M, Hansen H, Selin C, Hoffman EJ. Cardiac emission computed tomography: underestimation of regional tracer concentrations due to wall motion abnormalities. *J Comput Assist Tomogr* 1984;8:1063-1092.
 87. Hoffman EJ, Huang S-C, Phelps ME. Quantitation in positron emission computed tomography: I. Effects of object size. *J Comput Assist Tomogr* 1979;3:299-308.
 88. Gropler RJ, Siegel BA, Lee KJ, et al. Nonuniformity in myocardial accumulation of fluorine-18-fluorodeoxyglucose in normal fasted humans. *J Nucl Med* 1990;31:1749-1756.
 89. Berry JJ, Baker JA, Pieper KS, Hanson MW, Hoffman JM, Coleman RE. The effect of metabolic milieu on cardiac PET imaging using fluorine-18-deoxyglucose and nitrogen-13-ammonia in normal volunteers. *J Nucl Med* 1991;32:1518-1525.